Control Design for Safe Human-Robot Collaboration based on ISO/TS 15066 with Power and Force Limit

Ali Golshani[a], Afshin Kouhkord[b], Armin Ghanbarzadeh[b], Esmaeil Najafi[b]

[a]Faculty of Mechanical Engineering, University of Guilan, Rasht, Iran
[b]Faculty of Mechanical Engineering, K.N. Toosi University of Technology, Tehran, Iran
Emails: aligolshani96@yahoo.com, afshinkouhkord@yahoo.com, ghanbarzadeh.armin@gmail.com, najafi.e@kntu.ac.ir

***Abstract*—In collaborative robot systems, ensuring operator safety is crucial. This responsibility falls on robot integrators who must identify potential risks and design safety measures to prevent unwanted accidental contact with human operators. The ISO/TS 15066 guideline's Power and Force Limiting mode is instrumental in managing such incidents. This study explored the effectiveness of two control strategies, Sliding Mode Control and Computational Torque Control, within the framework of a six degrees of freedom robot manipulator, considering the design requirements of the power and force limiting mode. Simulation results showed that in the presence of external disturbances, Sliding Mode Controller outperformed in terms of response time, stability, and position tracking, making it more suitable for safety-focused applications in shared workspaces.**

***Index Terms*—Human Robot collaboration, ISO/TS 15066, Power and force limit, Safety, Sliding mode control, Computed torque control**

I. Introduction

Robotic manipulators, known for their precision, consistency, and durability, are becoming prevalent in modern industries, especially in high-volume manufacturing due to their high repeatability. Their adaptability to environmental changes enhances industrial productivity. These manipulators, capable of multitasking, integrate into assembly lines without requiring isolation, thereby improving spatial use and efficiency [1] [2]. Collaborative robots, often referred to as cobots, represent a novel category designed to work alongside human operators within shared workspaces. Cobots are capable of performing diverse tasks such as pick and place, machine tending, quality inspection, packaging, material handling, and welding, fostering a collaborative approach distinct from traditional industrial robots operating separately in controlled environments [3]. Fig. 1 shows the shared workspace for collaboration operations. Collaborative human-robot operations introduce unique safety challenges exceeding those of traditional factory robots, as highlighted in [4]. The International Organization for Standardization (ISO) has devised four practical modes for human-robot collaboration to mitigate these risks. Among them, the power and force limiting (PFL) mode reduces robot power and force to enhance safety during physical interaction

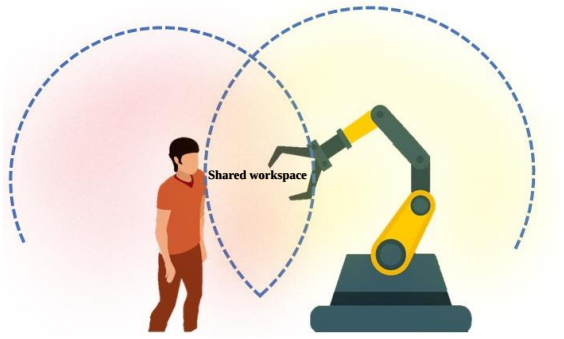

Fig. 1: Shared workspace between a robot and a human

without the need for physical barriers. Consequently, there is a critical need to establish quantifiable design standards for assessing unwanted physical contact, a central focus discussed in [5]. Numerous researchers have explored the correlation between factors like peak forces, stress, kinetic energy, and energy transfer to human tissues concerning injury occurrence and pain perception [5]. In [6] authors demonstrates the use of bruising as an injury indicator in human-robot collisions. Through real-person impact tests, researchers quantify the injury threshold and identify the force levels causing soft tissue bruising in [7]. The study tested varying impact levels, highlighting the need for advanced control strategies in collaborative robots for safety and efficiency. This includes sensor integration, machine learning, and motion planning to prevent collisions during task changes. In [8] researchers developed a model that uses online trajectory optimization which follows a model predictive control approach. In [9], a novel continuous adaptive control technique for SEA-driven robots in human-robot interactions is introduced. It includes two modes: "robot-in-charge," where the robot performs tasks independently with minimal human control, and "human-in-charge," where a human operator guides the robot's movements in a dominant role. Researchers in [10] proposed an end-user approach to collision detection and reaction for industrial manipulators. They used joint velocity references, motor currents, and joint positions

979-8-3503-0810-5/23/$31.00 ©2023 IEEE

to differentiate between accidental collisions and intended human-robot contacts. This approach enables collaboration mode activation and responsive robot behavior to human-applied forces. [11] presents a novel control approach for manipulating in dynamic situations and interacting physically with individuals while ensuring constraint compliance. In robotics control, Control Technique (CTC) and Sliding Mode Control (SMC) are two significant strategies. CTC focuses on tracking accuracy, reduced feedback reliance, compliance, and energy efficiency via Feedback Linearization. SMC is known for robustly handling nonlinear systems. Both methods contribute distinct strengths to robotics control [12]. This paper compares the performance of SMC and CTC on a robot manipulator similar to the Fanuc LR Mate 200iC, conforming to power and force limiting standards of ISO/TS 15066, using MATLAB simulations. The robot's end effector follows a predefined Bezier path in a shared workspace with a human operator, facing external torque disturbances. The goal is to compare the controllers' performance in managing disturbances while ensuring safety. The paper discusses the importance of ISO/TS 15066 in Human Robot Collaboration, introduces design requirements for PFL, and presents control strategies for SMC and CTM. A comparative analysis of the controllers is conducted, assessing the impact of disturbances on various parameters.

II. Safe Collaboration based on ISO/TS 15066 Standard

Human-robot collaboration is vital in manufacturing for complex tasks, as robots lack the intelligence to handle them. This collaboration improves efficiency but requires strict safety measures. Safety measures must be integrated into the design of robotic systems and collaborative workspaces to prioritize safety and minimize hazards [13]. The ISO/TS 15066 is essential for prioritizing safety and mitigating potential hazards in collaborative industrial robot systems. It establishes safety protocols, ensuring the safe coexistence of humans and robots in shared workspaces, with four defined collaborative methods.

1) hand guiding
2) safety-rated monitored stop
3) speed and separation monitoring
4) power and force limiting

Hand-guiding mode provides direct human control for intricate tasks, while safety-rated monitored stop mode halts robots when humans enter hazardous areas. Speed and separation monitoring ensures safety by slowing or stopping robots near humans. Vision systems aid in detection for SRMS and SSM modes, and power and force limiting allows physical interaction with operators [14].

Compared to SSM, PFL is a better option for collaboration as it does not require additional hardware. PFL limits kinetic energy transfer through velocity and force control, ensuring safety without extensive proximity sensors. It is a favorable choice when workspace awareness is limited. The method implementation depends on the terms of collaboration. [15]

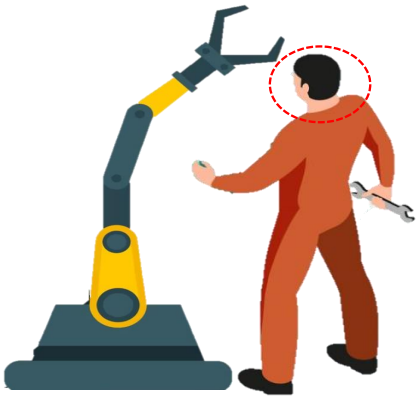

Fig. 2: Schematic of shared workspace , highlighting potential human-robot collisions according to PFL mode

In PFL mode, human-robot collisions are deemed acceptable, necessitating collaborative task design that ensures operator safety. This concept is well illustrated in Fig. 2. To ensure human collaborators, collaborative robot designs must minimize physical interaction severity to harmless levels [5]. The ISO/TS 15066's PFL mode establishes biomechanical limits for human-robot collisions using empirical research findings, defining maximum force and pressure levels that avoid pain or injury. It outlines twelve body zones for testing, each with corresponding limits for force, pressure, and speed [16] [17]. The standard distinguishes between transient and quasi-static contact based on their duration. Transient contact lasts less than 0.5 seconds, while quasi-static contact lasts longer. The standard sets speed limits to ensure collision forces and pressures during transient contact remain below pain thresholds for specific body parts. To determine the relative velocity of the end-effector, the standard uses a dot product of two vectors: V for the end-effector's velocity tangent to its path, and a unit vector describing the connection between the end-effector's position and a specific point on the human body. Fig. 3

Throughout the entire duration of the collaborative task, this relative speed should not exceed a specified maximum value. (1) indicates how to obtain the maximum relative speed of a robot value for each part of the body

$$
\begin{aligned}
V_{rel,max} &= \frac{F_{max}}{\sqrt{k\mu}} \\
\mu &= (\frac{1}{m_H} + \frac{1}{m_R})^{-}1 \\
m_R &= \frac{M}{2} + m_L,
\end{aligned}
\tag{1}
$$

where $Fmax$ represents the maximum contact force for specified body region, k represents the effective spring constant for specified body region, μ represents the reduced mass of the two-body system, m_R represents the effective mass of the robot manipulator, m_H represents the effective mass of the human body region , m_L represents the effective payload

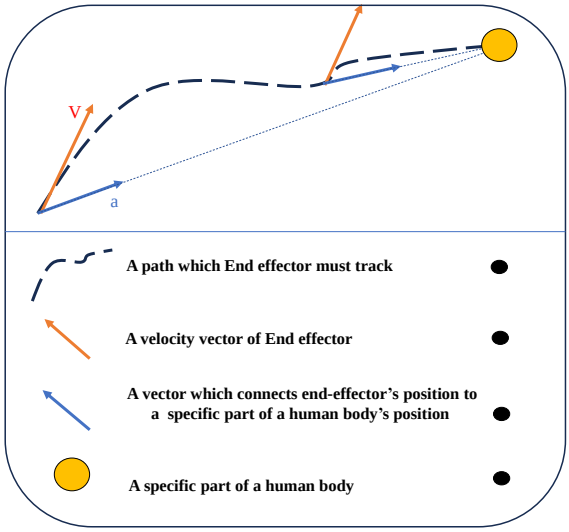

Fig. 3: Schematic of robot manipulator end-effector through its path

of the robot system and M represents the total mass of the moving parts of the end-effector.

In this study, we investigate the maximum relative velocity measurement for human forehead or skull and Table I provides details about forehead characteristics and the corresponding maximum relative velocity. Henceforth, we shall use the term "forehead" exclusively, omitting any reference to both the "forehead and skull".

TABLE I: Forehead characteristics and the corresponding maximum relative velocity

Body part	$\mathbf{F_{max}}$	k	$\mathbf{m_H}$	$\mathbf{m_L}$	$\mathbf{V_{rel,max}}$
Forehead	130(N)	150(N/mm)	4.4(kg)	0(kg)	0.1951(m/s)

III. Control Design

In this study we apply two control strategies to a robot manipulator with specifications similar to the Fanuc LR Mate 200ic series. The DH parameters of the robot were extracted from [18]. Also the physical parameters of the robot manipulator reported in Table II.

TABLE II: Robotic manipulator physical parameters

Link	Length (m)	Weight (kg)
1	0.3384	4.85331
2	0.3	7.9116
3	0.075	2.401
4	0.32	2.89084
5	0.08	0.043284

A. Trajectory planning

The desired path for the end-effector has been defined as a Bezier curve. Four control points (CP1, CP2, CP3 and CP4) in space have been carefully chosen in a way that the Bezier curve serves as the intended path within the workspace boundaries of the robot's end-effector.

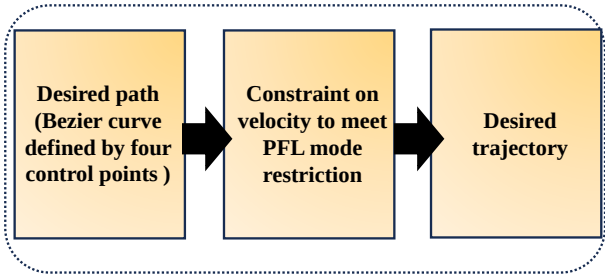

Fig. 4: Flowchart of generating the desired trajectory

The desired trajectory depends on which part of the human body is present in the shared workspace. As mentioned earlier, based on the PFL mode, the relative speed of the robot towards each part of the human body should not exceed a specified value (Which is equivalent to 0.1951 m/s in this case study). The desired trajectory corresponding to the Bezier path is calculated in a way that the relative speed of the end-effector with respect to human forehead are closely approximated to the permissible value throughout the simulation and do not exceed it Fig. 4. Using the desired numerical values of trajectory (x, y, z and t) determined by trajectory planning and curve fitting toolbox of MATLAB, the desired values over time were obtained. x, y, z indicate the desired position of end-effector in the Cartesian coordinate system and t represents time.

B. Computational Torque Control approach

Computed torque control stands as a potent approach in steering robotic manipulators along predefined trajectories, providing advantages such as improved tracking precision and reduced energy consumption by leveraging feedback linearization and an array of control techniques. However, its performance can be influenced by external disturbances [19].

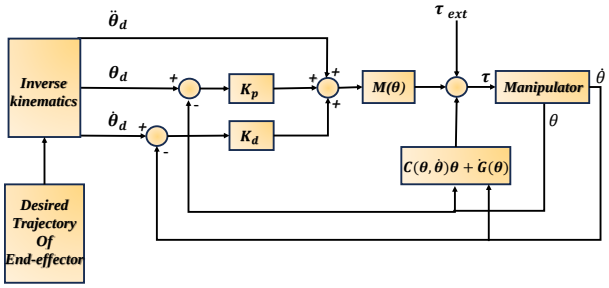

Fig. 5: Block diagram of Computational Torque Control

C. Sliding Mode Control approach

Sliding mode control (SMC) is a robust approach for managing system uncertainties and disturbances [20] [21]. Its main principle consists of creating a sliding surface (S) to guide the manipulator to the desired trajectory. In our study,

we adopt the classical sliding surface, which relies on a linear combination technique ($S = \dot{e} - \lambda e$). The control law in SMC is designed to guide the manipulator's state toward this surface. In various sources, $Ksign(S)$ has been commonly utilized as a control law, leading to the occurrence of chattering in robot control [22]. To eliminate chattering, researchers in [23] suggest replacing $\frac{2}{\pi}\arctan\left(\frac{2S}{\pi}\right)$ with $sign(S)$ in the control law. The alternative control law serves as a continuous approximation of $sign(S)$, which incorporates the arctangent function, ensuring smoother and uninterrupted control signals in contrast to the discontinuous sign function .

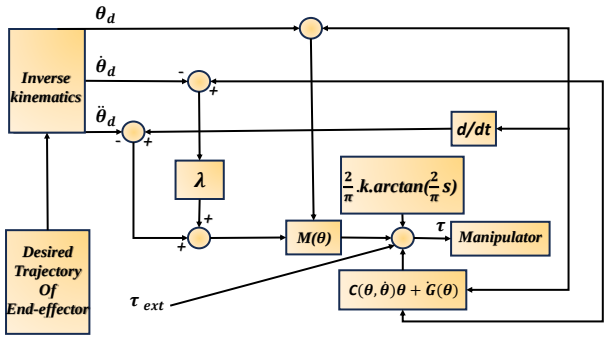

Fig. 6: Block diagram of sliding mode control

IV. Simulation Results

Using MATLAB, simulations were conducted for two distinct controllers: Computational Torque Control (CTC) and Sliding Mode Control (SMC). These simulations were executed under the assumption of the existence of external disturbances in the form of external torques. It is worth noting that, in terms of fair comparison, equivalent external torques were introduced into the manipulator as disturbances for both controllers. During time intervals ranging from one to two seconds and from four to four and a half seconds, external disturbances manifested as an extra torque equivalent to 1.1 times T , infiltrated both joint one and joint two where T is the torque vector corresponding to joint one and two (T= [T1 T2]), just before 1(s) and 4(s).

The desired relative velocity of the end effector with respect to the forehead was approximately considered to be almost 0.107 (m/s) throughout the path (except for the period from 4.8 seconds to 5 seconds. This is because the end effector passes in front of the forehead during this time interval, so the angle between the end effector's velocity and the unit vector connecting the end effector to the forehead is negative during this time).

Fig. 7 demonstrates the relative velocity of the end effector compared to the forehead using both controllers (SMC and CTC). Table III confirms that both controllers effectively maintained the relative velocity below the maximum limit of 0.1951 m/s throughout the entire path, while keeping it reasonably high.

Furthermore, Fig. 7 clearly illustrates that the SMC exhibits a quicker response in rectifying relative velocity errors and converging to the desired relative velocity compared to the CTC. This distinction becomes especially noteworthy in scenarios where, for instance, a substantial external disruption suddenly impacts the manipulator in the time interval of 1.5 to 2 seconds. During this time interval, SMC ensures that the actual end effector relative velocity closely aligns with the desired relative velocity. The SMC controller has a higher probability of keeping the relative velocity below the maximum threshold compared to the CTC controller when faced with another external disturbances, due to the shorter time interval for error correction. It's worth mentioning that in another case if actuators one and two experience an external torque of higher magnitude than what is currently being studied while following the same desired trajectory, the end effector's relative velocity can exceed the maximum allowable limit during the simulation. A more cautious strategy entails designing a desired trajectory in which the relative speed values of the actuator throughout the simulation time are lower than the case under study.

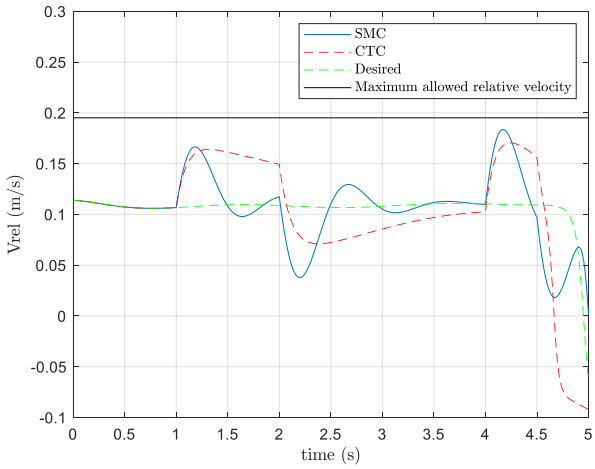

Fig. 7: Relative velocity of End effector with respect to Human forehead

TABLE III: Maximum value of End effector's relative velocity

	SMC	CTC
Maximum value (m/s)	0.183	0.17

Controllers in nonlinear systems face challenges due to nonlinearities and uncertainties. In this study the impact of the proposed disturbances is depicted in Fig. 8 and Fig. 9. The sliding mode controller demonstrates greater robustness against external disturbances compared to CTC, as it exhibits smaller sudden jumps (the zoomed parts) in control input. This observation highlights the superiority of sliding mode controllers over CTC by addressing the challenges posed by the external disturbances.

If we define the input error as the variation between the desired input without any disturbances (calculated using inverse dynamics) and the actual control input, accounting for the disturbances, Fig. 10 displays how this error evolves over

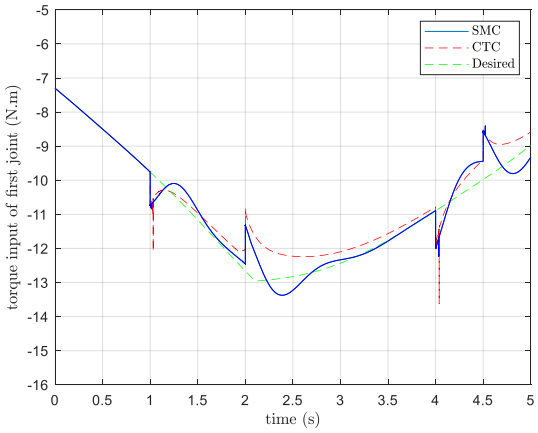

Fig. 8: SMC and CTC inputs of first actuator considering the presence of the external disturbances and the desired control input without any external disturbances

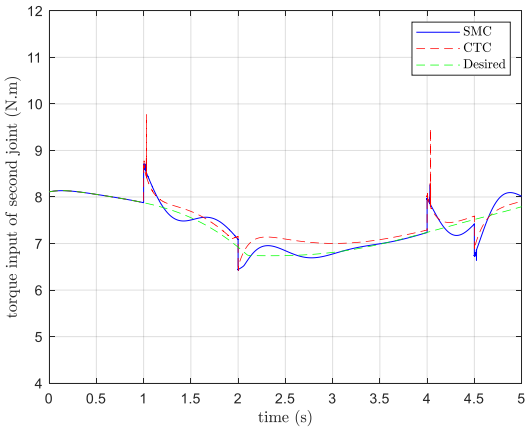

Fig. 9: SMC and CTC inputs of second actuator considering the presence of the external disturbances and the desired control input without any external disturbances

time of 2 seconds to 4 seconds where the robot manipulator responds to the first external disturbance. The significance of a controller's response time in mitigating input errors during external disturbance management is amplified when emphasizing safety as the foremost concern. A shorter response time for the input error in order to eliminate the external disturbance effect allows a quicker return to the desired input and trajectory. The significance here lies in the fact that the desired trajectory is designed in a way that the relative speed does not exceed a specified value. Therefore, tracking the desired trajectory and also the desired input as quickly as possible is considered an advantage.

Table IV and Table V provide numerical data about input error response times corresponding to the first actuator and the second actuator within the disturbance repulsion time of two to four seconds. According to Table IV for the first actuator SMC outperforms CTC in both rise time and settling time, suggesting that it can respond and stabilize more quickly when

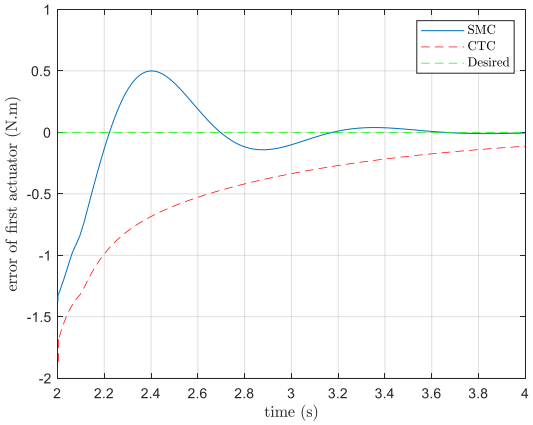

(a)

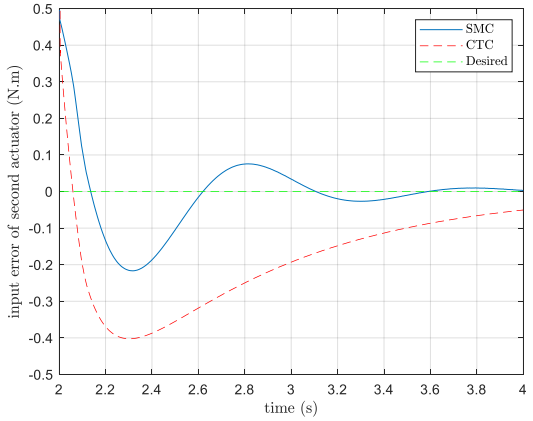

(b)

Fig. 10: Input error response to the external disturbance

TABLE IV: Response times of input error for the first actuator : Rise Time and Settling Time Analysis

	Rise time(s)	Settling Time(s)
SMC	0.18	1.51
CTC	1.13	1.57

the first external disturbance occurs.

TABLE V: Response times of input error for the second actuator : Rise Time and Settling Time Analysis

	Rise time(s)	Settling Time(s)
SMC	0.105	1.52
CTC	0.054	1.85

For the second actuator despite having a longer rise time, the SMC has a shorter settling time compared to the CTC indicating its faster stabilization following the first external disturbance (Table V).

Fig. 11 illustrates a shared workspace in the presence of the human forehead and the path taken by the end-effector.

Controller performance is crucial for tracking desired parameters while prioritizing safety. Table VI shows that the

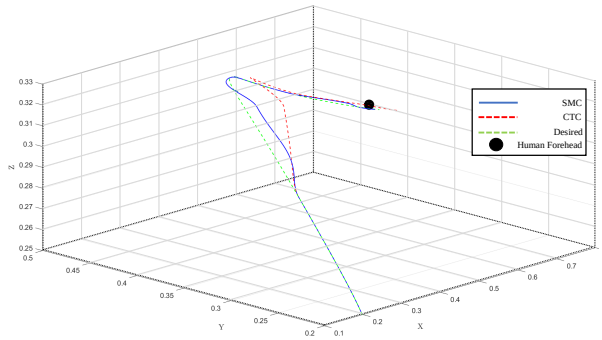

Fig. 11: The path followed by end-effector in presence of human forehead

TABLE VI

	$\int \lvert \mathbf{e_x} \rvert$	$\int \lvert \mathbf{e_y} \rvert$	$\int \lvert \mathbf{e_z} \rvert$
CTC	0.523	0.2579	0.009
SMC	0.195	0.0945	0.002

SMC controller outperforms the CTC controller in terms of accuracy, as it exhibits lower absolute error values for the end-effector along all three coordinate axes.

V. Conclusion

In this study, we analysed the performance of two controllers, sliding mode control (SMC) and computational torque control (CTC), for a robotic manipulator working near a human operator. Safety was prioritized using ISO/TS 15066's power and force limiting mode. The controllers effectively managed end-effector's relative velocity and adhered to safety limits in the presence of the external disturbances. However the Sliding Mode Controller exhibited rapid responses, ensuring quicker return to desired trajectories and better position tracking. Our findings highlight the importance of controller performance for safety in shared workspaces, making the Sliding Mode Controller a preferred choice.

References

[1] J. Corrales, G. G. Gomez, F. Torres, and V. Perdereau, "Cooperative tasks between humans and robots in industrial environments," *International Journal of Advanced Robotic Systems*, vol. 9, no. 3, p. 94, 2012.

[2] A. Kouhkord, A. Ghanbarzadeh, P. Ebrahimi, and E. Najafi, "Design of a genetic based optimized fuzzy logic controller for enhanced trajectory tracking accuracy of a 3p robot," in *2022 10th RSI International Conference on Robotics and Mechatronics (ICRoM)*. IEEE, 2022, pp. 497–502.

[3] H. Shin, K. Seo, and S. Rhim, "Allowable maximum safe velocity control based on human-robot distance for collaborative robot," in *2018 15th International Conference on Ubiquitous Robots (UR)*. IEEE, 2018, pp. 401–405.

[4] B. Matthias, S. Kock, H. Jerregard, M. Kallman, I. Lundberg, and R. Mellander, "Safety of collaborative industrial robots: Certification possibilities for a collaborative assembly robot concept," in *2011 IEEE International Symposium on Assembly and Manufacturing (ISAM)*. Ieee, 2011, pp. 1–6.

[5] B. Vemula, B. Matthias, and A. Ahmad, "A design metric for safety assessment of industrial robot design suitable for power-and force-limited collaborative operation," *International journal of intelligent robotics and applications*, vol. 2, no. 2, pp. 226–234, 2018.

[6] R. Behrens and N. Elkmann, "Study on meaningful and verified thresholds for minimizing the consequences of human-robot collisions," in *2014 IEEE International Conference on Robotics and Automation (ICRA)*. IEEE, 2014, pp. 3378–3383.

[7] G. T. Desmoulin and G. S. Anderson, "Method to investigate contusion mechanics in living humans," *Journal of forensic biomechanics*, vol. 2, 2011.

[8] M. Krämer, C. Rösmann, F. Hoffmann, and T. Bertram, "Model predictive control of a collaborative manipulator considering dynamic obstacles," *Optimal Control Applications and Methods*, vol. 41, no. 4, pp. 1211–1232, 2020.

[9] X. Li, Y. Pan, G. Chen, and H. Yu, "Adaptive human–robot interaction control for robots driven by series elastic actuators," *IEEE Transactions on Robotics*, vol. 33, no. 1, pp. 169–182, 2016.

[10] M. Geravand, F. Flacco, and A. De Luca, "Human-robot physical interaction and collaboration using an industrial robot with a closed control architecture," in *2013 IEEE International Conference on Robotics and Automation*. IEEE, 2013, pp. 4000–4007.

[11] M. Kimmel and S. Hirche, "Invariance control for safe human–robot interaction in dynamic environments," *IEEE Transactions on Robotics*, vol. 33, no. 6, pp. 1327–1342, 2017.

[12] R. ul Islam, J. Iqbal, and Q. Khan, "Design and comparison of two control strategies for multi-dof articulated robotic arm manipulator," *Journal of Control Engineering and Applied Informatics*, vol. 16, no. 2, pp. 28–39, 2014.

[13] P. Chemweno, L. Pintelon, and W. Decre, "Orienting safety assurance with outcomes of hazard analysis and risk assessment: A review of the iso 15066 standard for collaborative robot systems," *Safety Science*, vol. 129, p. 104832, 2020.

[14] O. I. de Normalización, *ISO-TS 15066: Robots and Robotic Devices: Collaborative Robots*. ISO, 2016.

[15] N. Lucci, B. Lacevic, A. M. Zanchettin, and P. Rocco, "Combining speed and separation monitoring with power and force limiting for safe collaborative robotics applications," *IEEE Robotics and Automation Letters*, vol. 5, no. 4, pp. 6121–6128, 2020.

[16] U. Dombrowski, T. Stefanak, and A. Reimer, "Simulation of human-robot collaboration by means of power and force limiting," *Procedia Manufacturing*, vol. 17, pp. 134–141, 2018.

[17] S. Robla-Gómez, V. M. Becerra, J. R. Llata, E. Gonzalez-Sarabia, C. Torre-Ferrero, and J. Perez-Oria, "Working together: A review on safe human-robot collaboration in industrial environments," *Ieee Access*, vol. 5, pp. 26 754–26 773, 2017.

[18] M. Abderrahmane, A. M. Djuric, W. Chen, and C. Yeh, "Study and validation of singularities for a fanuc lr mate 200ic robot," in *IEEE International Conference on Electro/Information Technology*. IEEE, 2014, pp. 432–437.

[19] C. Chen, C. Zhang, T. Hu, H. Ni, and W. Luo, "Model-assisted extended state observer-based computed torque control for trajectory tracking of uncertain robotic manipulator systems," *International Journal of Advanced Robotic Systems*, vol. 15, no. 5, p. 1729881418801738, 2018.

[20] B. Zhang, X. Yang, D. Zhao, S. K. Spurgeon, and X. Yan, "Sliding mode control for nonlinear manipulator systems," *IFAC-PapersOnLine*, vol. 50, no. 1, pp. 5127–5132, 2017.

[21] N. Y. Lademakhi, R. Shiri, A. Korayem, S. Nekoo, and Z. Fazilati, "Superiority of finite time sdre and non-singular terminal smc controller for n-dof manipulators," in *2018 6th RSI International Conference on Robotics and Mechatronics (IcRoM)*. IEEE, 2018, pp. 315–321.

[22] N. Nasiri and N. Y. Lademakhi, "Nonlinear combined smc-sdre control versus smc and sdre approaches for electrical flexible-joint robots based on optimal observer," in *2021 9th RSI International Conference on Robotics and Mechatronics (ICRoM)*. IEEE, 2021, pp. 568–573.

[23] F. Shokouhi and A.-H. Davaie Markazi, "A new continuous approximation of sign function for sliding mode control," in *International Conference on Robotics and Mechantronics (ICRoM 2018). Tehran. Iran*, 2018.